Table 2. Identification of patients with *CNGA1* sequence mutations and variants in this study.

Family ID	Exon	Nucleotide Change	Amino Acid Change	State	Frequency*	Polyphen-2 (score)	SIFT (score)	SNP ID	Reference	Pathogenicity
RP#002	5	c.191delG	p.G64Vfs29X	Homo	2				HGVB	Disease-causing
RP#019	6	c.265delC	p.L89FfsX4	Hetero	2				Chen et al. 2013	Disease-causing
	11	c.1429delG	p.V477YfsX17	Hetero	0				This study	
RP#021	5	c.191delG	p.G64Vfs29X	Homo	2				HGVB	Disease-causing
RP#029	6	c.265delC	p.L89FfsX4	Homo	2				Chen et al. 2013	Disease-causing
RP#040	11	c.G1271A	p.R424Q	Hetero	7	Benign (0.266)	Damaging (0)	rs192912733	Jin et al. 2008	Not disease-causing
RP#063	11	c.G2042C	p.G681A	Hetero	1	Benign (0.001)	Tolerated (0.36)		HGVB	Not disease-causing
RP#087	11	c.G860A	p.R287K	Hetero	5	Benign (0.101)	Tolerated (0.32)		HGVB	Not disease-causing
RP#094	6	c.265delC	p.L89FfsX4	Homo	2				Chen et al. 2013	Disease-causing

Polyphen-2 (http://genetics.bwh.harvard.edu/pph2/); SIFT (http://sift.jcvi.org); HGVB = Human Genetic Variation Browser (http://www.genome.med.kyoto-u.ac.jp/SnpDB/about.html); Frequency* show the number of mutations or variants found in 1150 alleles of 575 controls.

doi:10.1371/journal.pone.0108721.t002

of known and predicted arRP-causing mutations; and third, homozygosity or compound heterozygosity of predicted arRP-causing mutations. Mutations were defined as disease causing only if these criteria were fulfilled. Mutations causing exon truncation through frameshift, splicing and termination were considered to be more severe than missense mutations with unknown pathogenic relevance. In addition, to investigate the potential disease-causing variants, we added three genetic criteria: first, compound heterozygosity of known arRP-causing mutation and missense potential arRP-causing variant; second, compound heterozygosity of predicted arRP-causing mutation and potential arRP-causing variant; and third, homozygosity or compound heterozygosity of potential arRP-causing variants.

Direct sequencing of the *CNGA1* gene

The *CNGA1* mutations identified by whole exome sequencing were further confirmed by direct sequencing. An additional 69 arRP/spRP patients were analyzed by direct sequencing for all coding exons (4 to 11) of *CNGA1*. The targeted exons (4 to 11) of the *CNGA1* gene were amplified by PCR using the primer pairs given in Table S2 in File S1. The PCR products were purified using Agencourt APMure XP (Beckman Coulter, Brea, CA) and used as a template for sequencing. Both DNA strands were sequenced by an automated sequencer (3730*xl* DNA Analyzer; Life Technologies Corporation, Carlsbad, CA) using the BigDye Terminator kit V3.1 (Life Technologies Corporation).

Assessment of found mutations or variants in this study

Novel mutations and variants were defined as those not present in the literature, dbSNP database (http://www.ncbi.nlm.nih.gov/SNP/), Human Genetic Variation Browser, 1000 Genome project database or the Human Gene Mutation Database (http://www.hgmd.cf.ac.uk). In addition, the frequency of identified mutations or variants in this study was investigated using in-house exome sequencing data from 575 unaffected Japanese controls at Yokohama City University. Segregation was confirmed for both the arRP-causing mutations and potential arRP-causing variants by direct sequencing when parent samples were available.

Results

Whole exome sequencing analysis and identification of frequent arRP gene mutations

To identify frequent arRP-causing genes, we performed whole exome sequencing in non-syndromic 30 arRP/spRP patients. We focused on 212 retinal disease-causing genes registered in RetNet database updated on March 10, 2014. The average of mean depth for all 30 samples reached 71.11±7.68-fold and the average of coverage at 4- and 12-fold for all 30 samples reached 98.1% and 92.5% respectively. The analysis of arRP-causing mutations and potential arRP-causing variants was conducted according to the criteria described in Materials and Methods. Segregation of identified arRP-causing mutations and potential arRP-causing variants were conducted in five families: RP#002, RP#004, RP#011, RP#016 and RP#019. Although the results of segregation in RP#002, RP#004, RP#016 and RP#019 matched the inheritance pattern, two *USH2A* variants in RP#011 (Table S1 in File S1) did not match the inheritance pattern because the father of RP#011 carried two identical *USH2A* variants. Therefore, we concluded that the two *USH2A* variants in RP#011 were not arRP-causing. Consequently, the exome analysis identified eight arRP-causing mutations including three novel mutations and five known mutations in eight arRP/spRP patients [6,16,26,27] and identified potential arRP-causing

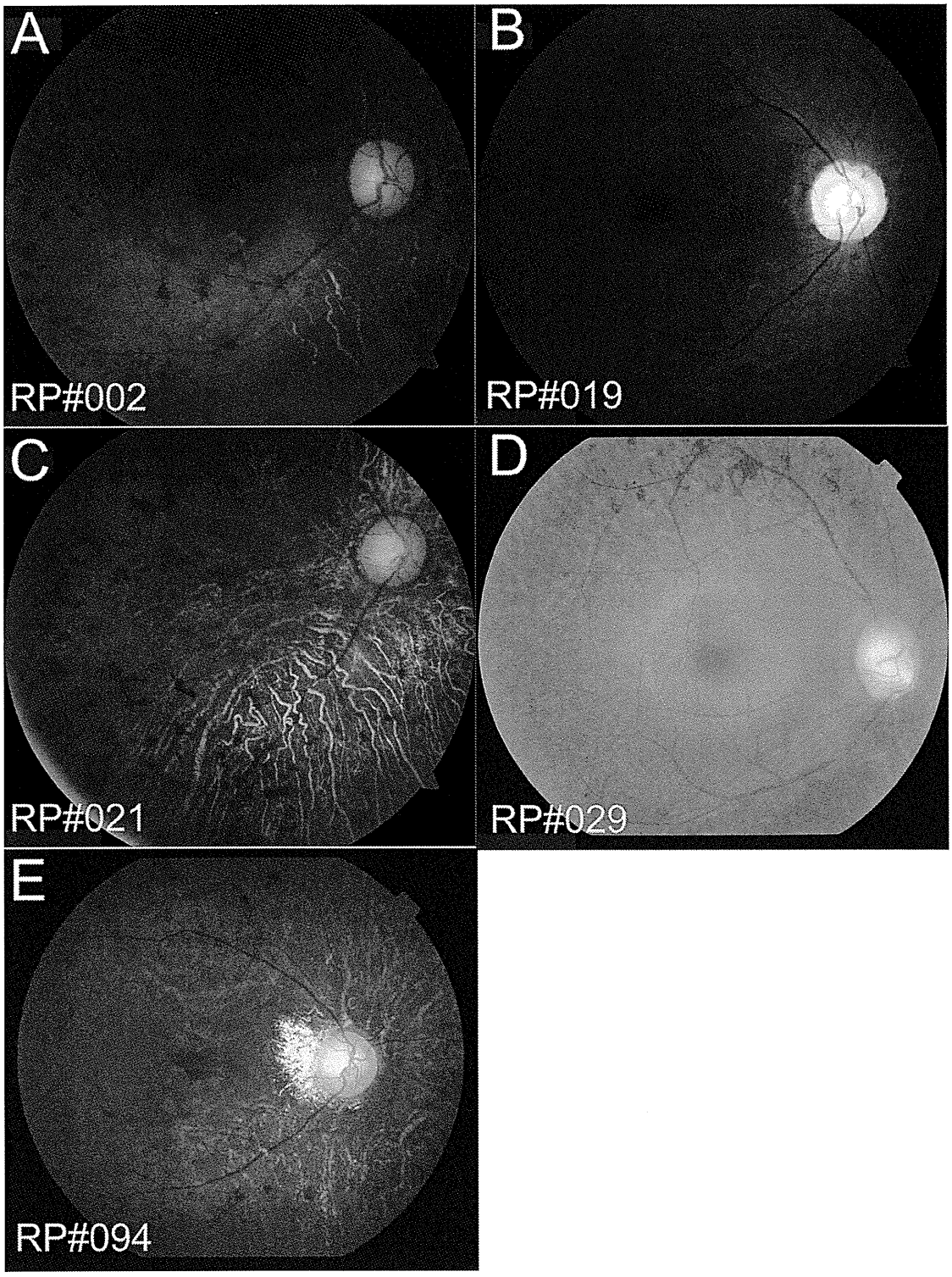

Figure 3. Fundus photographs of the patients with heterozygous or homozygous *CNGA1* mutations. Funduscopy indicates retinal degeneration with pigmentation and attenuation of retinal vessels in all patients. Macular edema does not existed in any patient, although retinal degeneration in the macular region is observed in RP#002, RP#021 and RP#094 (A, C and E).
doi:10.1371/journal.pone.0108721.g003

variants including six novel variants and five known variants in five arRP/spRP patients (Table 1). The arRP-causing mutations were found in *CNGA1* (four patients), *EYS* (three patients) and S-antigen retina and pineal gland (*SAG*) (one patient). Potential arRP-casing variants were found in *USH2A* (two patients), *EYS* (one patient), tubby like protein 1 (*TULP1*) (one patient) and chromosome 2 open reading frame 71 (*C2orf71*) (one patient). Among these genes, the most frequent arRP-causing gene was

Table 3. Ophthalmic findings in five patients with retinitis pigmentosa with compound heterozygous or homozygous *CNGA1* mutations.

Patient	Diagnosed Age, Examined Age, Sex	Onset of night blindness	BCVA		ERG	Visual field	Mutations
			Right	Left			
RP#002	42, 51, M	Childhood	0.5	0.7	Non-recordable	Severely constricted	c.191delG/c.191delG
RP#019	26, 35, F	Childhood	1.0	1.0	Non-recordable	Ring scotoma	c.265delC/c.1429delG
RP#021	60, 65, M	Childhood	0.2	0.1	Non-recordable	Severely constricted	c.191delG/c.191delG
RP#029	25, 51, F	Childhood	1.0	1.0	Non-recordable	Severely constricted	c.265delC/c.265delC
RP#094	16, 46, M	Childhood	0.4	0.3	Non-recordable	Severely constricted	c.265delC/c.265delC

BCVA = decimal corrective visual acuity; ERG = electroretinography; M = male; F = female.

doi:10.1371/journal.pone.0108721.t003

CNGA1. In particular, pedigree RP#002 with a homozygous c.191delG (p.G64VfsX29) mutation, RP#019 with compound heterozygous c.265delC (p.L89FfsX4) and c.1429delG (p.V477YfsX17) mutations, RP#021 with a homozygous c.191delG mutation and RP#029 with a homozygous c.265delC mutation were identified. Further direct sequencing confirmed that the parents in pedigree RP#019 had c.265delC or c.1429delG respectively. The *CNGA1* sequence was compared with the NCBI reference sequence for the *CNGA1* transcript (GenBank ID; NM_000087.3).

Screening of all *CNGA1* exons in 69 additional arRP/spRP Japanese patients

Direct sequencing of the coding region of the *CNGA1* gene in 69 arRP/spRP patients identified homozygous c.265delC mutation in pedigree RP#094 and three heterozygous variants c.G860A (p.R287K), c.G1271A (p.R424Q) and c.G2042C (p.G681A) in pedigrees RP#040, RP#063 and RP#087 respectively. All pedigrees identified to have arRP-causing mutations or potential arRP-causing variants are shown in Figure 1.

Identified *CNGA1* mutations and variants

Among the three arRP-causing mutations and three variants found in this study, two (c.265delC and c.G1271A) were previously reported as arRP-causing or potential arRP-causing [11,26] and four were not reported as arRP-causing or potential arRP-causing (c.191delG, c.265delC, c.G860A and c.G2042C). The polyphen-2 program predicted that all three missense variants in p.R287K (c.G860A), p.R424Q (c.G1271A) and p.G681A (c.G2042C) were benign. In contrast, the SIFT program predicted that p.R424Q (c.G1271A) potentially could cause severe damage to the protein, whereas p.G681A (c.G2042C) and p.R287K (c.G860A) potentially could cause mild damage. All identified mutations and variants in *CNGA1* gene are summarized in Table 2 and sequence data are given in Figure 2.

Haplotype analysis

The haplotypes of *CNGA1* and the surrounding sequences were determined for four arRP patients, RP#002, RP#019, RP#021 and RP#029. Single-nucleotide polymorphisms (SNPs) with a frequency higher than 5% (1000 Genomes project database) were determined within 1 kb upstream and downstream of *CNGA1* (chromosome 4, positions 47,937,994–48,014,961) as shown in Table S3 in File S1. The haplotype analysis determined an identical haplotype for four alleles in patients RP#002 and RP#021 suggesting a common ancestor for the c.191delG mutation. Moreover, identical haplotypes for one allele in patient RP#019 and for both alleles in patient RP#029 were detected suggesting a common ancestor for the c.265delC mutation.

Clinical features of *CNGA1* mutations

To characterize the clinical features of patients with *CNGA1* mutations, we additionally investigated the clinical data of five patients with compound heterozygous or homozygous *CNGA1* mutations (Table 3). All five patients reported that they noticed night blindness from childhood. Funduscopy showed retinal degeneration with pigmentation and attenuation of retinal vessels in all patients (Fig. 3). Macular edema was not observed in any patients, although retinal degeneration in macular regions was detected in RP#002, RP#021 and RP#094 (Fig. 3A, 3C and 3E). The BCVA of RP#019 and RP#029 remained at 1.0, whereas that of RP#002, RP#021 and RP#094 was reduced. ERG showed no recordable pattern in four patients and could not

be conducted in one patient. The GP of RP#022 showed ring scotoma with a preserved peripheral visual field, whereas that of another four patients was severely constricted.

Discussion

Mutations in the *CNGA1* gene were identified for the first time in a Japanese population with a high frequency of 5.1% for homozygous or compound heterozygous mutations. The exome analysis of arRP/spRP patients revealed that 43.3% carried arRP-causing mutations or potential arRP-causing variants in *CNGA1* (13.3%), *EYS* (13.3%), *USH2A* (6.7%), *C2orf71* (3.3%), *SAG* (3.3%) and *TULP1* (3.3%). Although the prevalence of other five gene mutations was consistent with that in previous studies [1,4–8,28–30], the prevalence of *CNGA1* was clearly higher than in population of European descent [31,32]. We screened for mutation in all the coding exons of *CNGA1* in an additional 69 arRP/spRP Japanese patients to further investigate the prevalence of *CNGA1* mutations in the Japanese population. We identified an arRP-causing homozygous *CNGA1* mutation in one patient. Consequently, three *CNGA1* frameshift mutations (c.191delG, c.265delC and c.1429delG) were identified as arRP-causing mutations in five patients (Table 2).

Rod cyclic nucleotide-gated ion channels contain CNGA1 and CNGB1 protein at a ratio of 3 CNGA1:1 CNGB1 [33]. Each molecule of CNGA1 protein has at least three functional domains as described in the UniProtKB (acc. # P29973, http://www.uniprot.org, Cross-References, ProteinModelPortal); these domains function as a cation-transporter domain (residues 202–396, the Pfam ion_trans motif, http://pfam.sanger.ac.uk), cGMP-binding domain (residues 404–596, SWISSMODEL structure based on the PDB file: 4hbn_A, http://www.rcsb.org/pdb/home/home.do) and carboxy-terminal leucine zipper (CLZ) domain (residues 623–690, experimental structure based on the PDB file:3swf). The p.G64VfsX29 (c.191delG) and p.L89FfsX4 (c.265delC) protein had no transmembrane lesions, and most of the protein structure including all three functional domains was abolished. In contrast, the p.V477YfsX17 (c.1429delG) mutant protein had the correct structure up to 5th transmembrane domain helix, but lacked the 6th transmembrane domain helix, the cGMP-binding site, and the coiled-coil CLZ domain. The cGMP-binding site is important for the function of CNGA1 as a cation channel. Loss of the cGMP-binding site is likely to influence the final stage of the photo transduction pathway [31]. In addition, the absence of the coiled-coil CLZ domain completely disrupts the 3:1 stoichiometry in CNG channels [33]. Although the p.V477YfsX17 (c.1429delG) mutant may retain part of its structure, the protein function is predicted to be completely lost.

We additionally identified the heterozygous *CNGA1* missense variants c.G860A (p.R287K), c.G1271A (p.R424Q) and c.G2042C (p.G681A) (Table 2). Heterozygous c.G1271A variant has been previously reported [11]. Based on the mild score given by the polyphen-2 program and the severe score given by the SIFT program, we also predicted that this variant is potentially disease causing. In contrast, the two novel missense variants c.G860A and c.G2042C were predicted to cause mild damage by both the polyphen-2 and SIFT programs suggesting that it is non-pathogenic. Overall, all three missense *CNGA1* variants (c.G860A, c.G1271A and c.G2042C) were found in only one allele of *CNGA1*. We conclude that these three *CNGA1* variants were not disease causing in nature, at least from the phenotypic observation.

The clinical course of the five patients with compound heterozygous or homozygous *CNGA1* mutations included night blindness from childhood, visual field loss in middle age, non-recordable ERG and characteristic retinal degeneration pattern of RP, which were consistent with previously reported phenotypes of *CNGA1* mutations [32,34]. Retinal degeneration in the macular region and severely decreased BCVA occurred in 3/5 patients suggesting that the advanced stage of *CNGA1* mutations included degeneration of the entire retina with both rod and cone photoreceptors. Although the genotype-phenotype correlation for *CNGA1* mutations was not clear in this study, all five patients with *CNGA1* mutations showed typical phenotypes of RP.

Previous reports have shown a strong association of *CNGA1* with arRP [11,26,31,32,34,35]. Dryja et al. estimated the prevalence of *CNGA1* mutations in arRP patients to be between 1.7 and 2.3% (3 or 4 of 173 patients) [31]. The prevalence of *CNGA1* mutations in a Spanish arRP population was 2.1% (1 of 46 patients) [32], whereas that in a Chinese population with hereditary retinal dystrophy was 4.0% (1 of 25 patients) [26]. The average prevalence of *CNGA1* mutations in arRP/spRP patients was 7.6% (1 of 13 patients) [26]. These findings suggest that the prevalence of *CNGA1* mutations is higher in Asian population than in populations of European descent. The prevalence of *CNGA1* mutations in Chinese populations requires further study because only one Chinese patient has been reported to have a homozygous mutation in this gene [26]. Jin et al. investigated *CNGA1* exons 6, 8 and partial 11 in 193 Japanese RP families and found a single heterozygous *CNGA1* variant (c.1271G>A) [11]. In our study, all coding exons of *CNGA1* were screened and the estimate prevalence of *CNGA1* mutations reached at 5.1% (5 of 99 patients) including four homozygous and one compound heterozygous patients. Our findings suggest that the prevalence of *CNGA1* mutations is higher in Asian populations than in European populations. Moreover, c.191delG mutation has only been reported in Human Genetic Variation Browser (the database of genetic variations in Japanese population, http://www.genome.med.kyoto-u.ac.jp/SnpDB/), c.265delC mutation only reported in Chinese population [26] and c.1429delG mutation identified as novel. The *CNGA1* mutations found in this study only overlapped with mutations identified in studies of Asian individuals indicating that the founder is specific to Asian populations. Lastly, the haplotypes for the *CNGA1* mutations found in this study were individually unique (Table S3 in File S1). Further investigation of haplotypes is required to clarify the origin of these *CNGA1* mutations.

Supporting Information

File S1 Supporting Tables. Table S1, All rare variants of 30 arRP/spRP paients of this study, focusing on 212 retinal disease-causing genes registered in the Retinal Information Network (https://sph.uth.edu/retnet/). Table S2, *CNGA1* primers and PCR conditions. Table S3, Haplotype analysis of four retinitis pigmentosa patients with *CNGA1* mutations.
(DOC)

Acknowledgments

We thank the patients and their families for participation in this study. The authors wish to acknowledge RIKEN GeNAS for the sequencing of the exome-enriched libraries using the Illumina HiSeq2000.

Author Contributions

Conceived and designed the experiments: TI SK. Performed the experiments: SK MA YS KY KI MF TH MK SU KT KS KK YT NM. Analyzed the data: SK MA TI. Contributed reagents/materials/analysis tools: HT. Wrote the paper: SK TI.

References

1. Hartong DT, Berson EL, Dryja TP (2006) Retinitis pigmentosa. Lancet 368: 1795–1809.
2. Mansergh FC, Millington-Ward S, Kennan A, Kiang AS, Humphries M, et al. (1999) Retinitis pigmentosa and progressive sensorineural hearing loss caused by a C12258A mutation in the mitochondrial MTTS2 gene. Am J Hum Genet 64: 971–985.
3. Kajiwara K, Berson EL, Dryja TP (1994) Digenic retinitis pigmentosa due to mutations at the unlinked peripherin/*RDS* and *ROM1* loci. Science 264: 1604–1608.
4. Rivolta C, Sweklo EA, Berson EL, Dryja TP (2000) Missense mutation in the *USH2A* gene: association with recessive retinitis pigmentosa without hearing loss. Am J Hum Genet 66: 1975–1978.
5. Abd El-Aziz MM, Barragan I, O'Driscoll CA, Goodstadt L, Prigmore E, et al. (2008) *EYS*, encoding an ortholog of Drosophila spacemaker, is mutated in autosomal recessive retinitis pigmentosa. Nat Genet 40: 1285–1287.
6. Collin RW, Littink KW, Klevering BJ, van den Born LI, Koenekoop RK, et al. (2008) Identification of a 2 Mb human ortholog of Drosophila eyes shut/spacemaker that is mutated in patients with retinitis pigmentosa. Am J Hum Genet 83: 594–603.
7. Abd El-Aziz MM, O'Driscoll CA, Kaye RS, Barragan I, El-Ashry MF, et al. (2010) Identification of novel mutations in the ortholog of Drosophila eyes shut gene (*EYS*) causing autosomal recessive retinitis pigmentosa. Invest Ophthalmol Vis Sci 51: 4266–4272.
8. Audo I, Sahel JA, Mohand-Said S, Lancelot ME, Antonio A, et al. (2010) *EYS* is a major gene for rod-cone dystrophies in France. Hum Mutat 31: E1406–1435.
9. Bandah-Rozenfeld D, Littink KW, Ben-Yosef T, Strom TM, Chowers I, et al. (2010) Novel null mutations in the *EYS* gene are a frequent cause of autosomal recessive retinitis pigmentosa in the Israeli population. Invest Ophthalmol Vis Sci 51: 4387–4394.
10. Klevering BJ, Yzer S, Rohrschneider K, Zonneveld M, Allikmets R, et al. (2004) Microarray-based mutation analysis of the *ABCA4* (*ABCR*) gene in autosomal recessive cone-rod dystrophy and retinitis pigmentosa. Eur J Hum Genet 12: 1024–1032.
11. Jin ZB, Mandai M, Yokota T, Higuchi K, Ohmori K, et al. (2008) Identifying pathogenic genetic background of simplex or multiplex retinitis pigmentosa patients: a large scale mutation screening study. J Med Genet 45: 465–472.
12. Fujiki K, Hotta Y, Hayakawa M, Sakuma H, Shiono T, et al. (1992) Point mutations of rhodopsin gene found in Japanese families with autosomal dominant retinitis pigmentosa (ADRP). Jpn J Hum Genet 37: 125–132.
13. Saga M, Mashima Y, Akeo K, Oguchi Y, Kudoh J, et al. (1994) Autosomal dominant retinitis pigmentosa. A mutation in codon 181 (Glu–>Lys) of the rhodopsin gene in a Japanese family. Ophthalmic Genet 15: 61–67.
14. Fujiki K, Hotta Y, Murakami A, Yoshii M, Hayakawa M, et al. (1995) Missense mutation of rhodopsin gene codon 15 found in Japanese autosomal dominant retinitis pigmentosa. Jpn J Hum Genet 40: 271–277.
15. Hosono K, Ishigami C, Takahashi M, Park DH, Hirami Y, et al. (2012) Two novel mutations in the *EYS* gene are possible major causes of autosomal recessive retinitis pigmentosa in the Japanese population. PLoS One 7: e31036.
16. Iwanami M, Oshikawa M, Nishida T, Nakadomari S, Kato S (2012) High prevalence of mutations in the *EYS* gene in Japanese patients with autosomal recessive retinitis pigmentosa. Invest Ophthalmol Vis Sci 53: 1033–1040.
17. Shendure J, Ji H (2008) Next-generation DNA sequencing. Nat Biotechnol 26: 1135–1145.
18. Mardis ER (2008) The impact of next-generation sequencing technology on genetics. Trends Genet 24: 133–141.
19. Mardis ER (2008) Next-generation DNA sequencing methods. Annu Rev Genomics Hum Genet 9: 387–402.
20. Ansorge WJ (2009) Next-generation DNA sequencing techniques. N Biotechnol 25: 195–203.
21. Shanks ME, Downes SM, Copley RR, Lise S, Broxholme J, et al. (2013) Next-generation sequencing (NGS) as a diagnostic tool for retinal degeneration reveals a much higher detection rate in early-onset disease. Eur J Hum Genet 21: 274–280.
22. Berson EL (1993) Retinitis pigmentosa. The Friedenwald Lecture. Invest Ophthalmol Vis Sci 34: 1659–1676.
23. Katagiri S, Yoshitake K, Akahori M, Hayashi T, Furuno M, et al. (2013) Whole-exome sequencing identifies a novel *ALMS1* mutation (p.Q2051X) in two Japanese brothers with Alström syndrome. Molecular Vision 19: 2393–2406.
24. Li H, Durbin R (2009) Fast and accurate short read alignment with Burrows-Wheeler transform. Bioinformatics 25: 1754–1760.
25. McKenna A, Hanna M, Banks E, Sivachenko A, Cibulskis K, et al. (2010) The Genome Analysis Toolkit: a MapReduce framework for analyzing next-generation DNA sequencing data. Genome Res 20: 1297–1303.
26. Chen X, Zhao K, Sheng X, Li Y, Gao X, et al. (2013) Targeted sequencing of 179 genes associated with hereditary retinal dystrophies and 10 candidate genes identifies novel and known mutations in patients with various retinal diseases. Invest Ophthalmol Vis Sci 54: 2186–2197.
27. Fuchs S, Nakazawa M, Maw M, Tamai M, Oguchi Y, et al. (1995) A homozygous 1-base pair deletion in the arrestin gene is a frequent cause of Oguchi disease in Japanese. Nat Genet 10: 360–362.
28. Hagstrom SA, North MA, Nishina PL, Berson EL, Dryja TP (1998) Recessive mutations in the gene encoding the tubby-like protein TULP1 in patients with retinitis pigmentosa. Nat Genet 18: 174–176.
29. Nakazawa M, Wada Y, Tamai M (1998) Arrestin gene mutations in autosomal recessive retinitis pigmentosa. Arch Ophthalmol 116: 498–501.
30. Collin RW, Safieh C, Littink KW, Shalev SA, Garzozi HJ, et al. (2010) Mutations in *C2ORF71* cause autosomal-recessive retinitis pigmentosa. Am J Hum Genet 86: 783–788.
31. Dryja TP, Finn JT, Peng YW, McGee TL, Berson EL, et al. (1995) Mutations in the gene encoding the alpha subunit of the rod cGMP-gated channel in autosomal recessive retinitis pigmentosa. Proc Natl Acad Sci U S A 92: 10177–10181.
32. Paloma E, Martinez-Mir A, Garcia-Sandoval B, Ayuso C, Vilageliu L, et al. (2002) Novel homozygous mutation in the alpha subunit of the rod cGMP gated channel (*CNGA1*) in two Spanish sibs affected with autosomal recessive retinitis pigmentosa. J Med Genet 39: E66.
33. Shuart NG, Haitin Y, Camp SS, Black KD, Zagotta WN (2011) Molecular mechanism for 3:1 subunit stoichiometry of rod cyclic nucleotide-gated ion channels. Nat Commun 2: 457.
34. Zhang Q, Zulfiqar F, Riazuddin SA, Xiao X, Ahmad Z, et al. (2004) Autosomal recessive retinitis pigmentosa in a Pakistani family mapped to CNGA1 with identification of a novel mutation. Mol Vis 10: 884–889.
35. Gonzalez-del Pozo M, Borrego S, Barragan I, Pieras JI, Santoyo J, et al. (2011) Mutation screening of multiple genes in Spanish patients with autosomal recessive retinitis pigmentosa by targeted resequencing. PLoS One 6: e27894.

Clinical Ophthalmology

Dovepress
open access to scientific and medical research

Open Access Full Text Article

CASE SERIES

Clinical course of focal choroidal excavation in Vogt–Koyanagi–Harada disease

Yuko Nishikawa[1–3,*]
Kaoru Fujinami[1,2,4,5,*]
Ken Watanabe[1,2]
Toru Noda[1,2]
Kazushige Tsunoda[1,2]
Kunihiko Akiyama[1,2]

[1]Department of Ophthalmology, National Hospital Organization, Tokyo Medical Center, Tokyo, Japan; [2]Laboratory of Visual Physiology, National Institute of Sensory Organs, National Tokyo Medical Center, Tokyo, Japan; [3]Department of Ophthalmology, Osaka Medical College, Takatsuki, Osaka, Japan; [4]Department of Ophthalmology, Keio University School of Medicine, Tokyo, Japan; [5]UCL Institute of Ophthalmology, London, UK

*These authors contributed equally to this work

Abstract: We describe focal choroidal excavation (FCE) in a case of Vogt–Koyanagi–Harada (VKH) disease and compare the findings with different chorioretinal conditions. A 55-year-old man was diagnosed with VKH based on panuveitis and exudative retinal detachments. Spectral-domain optical coherence tomography demonstrated a dome-shaped protrusion with a nonconforming pattern at the fovea, which had been detected as a conforming pattern 1 year before the onset. The FCE pattern returned into a conforming pattern following corticosteroid therapy. These findings suggest that the natively existent FCE could be affected by pathophysiological changes of VKH as well as other chorioretinal conditions.

Keywords: choroidal excavation, focal choroidal excavation, Vogt–Koyanagi–Harada disease, optical coherence tomography

Introduction

Focal choroidal excavation (FCE) was first described by Jampol et al[1] as an anomalous excavation of the choroid; it is typically observed by optical coherence tomography (OCT).[1,2] This condition has been associated with several chorioretinal conditions and asymptomatic status, including central serous chorioretinopathy, choroidal neovascularization, and best vitelliform macular dystrophy.[1–12] However, the mechanisms underlying the formation of FCE remain uncertain.

Wakabayashi et al[2] described two patterns of FCE: 1) conforming pattern – excavations that involved the outer retinal layers up to and including the external limiting membrane; and 2) nonconforming pattern – excavations that involved only the retinal pigment epithelium (RPE).

Recently, a case report of FCE associated with Vogt–Koyanagi–Harada (VKH) disease has been published,[13] which documented cross-sectional observation. Here we describe a clinical course of FCE associated with VKH before and after treatment and compare the morphological findings of FCE in four subjects with different chorioretinal conditions.

Case report

A 55-year-old man (subject 1) presented with bilateral metamorphopsia, with decimal visual acuity being 0.8 in the right eye and 1.2 in the left. The clinical diagnosis of VKH was made based on bilateral panuveitis and multifocal exudative retinal detachments at the posterior poles (Figure 1). High-dose corticosteroid therapy with gradual tapering was initiated 3 days after presentation. The serous detachments entirely resolved within 9 weeks and visual acuity in the right eye improved to 1.2.

Serial spectral-domain OCT (SD-OCT) images obtained at the preuveitic, uveitic, and posttreatment phase are shown in Figure 2. SD-OCT obtained 1 year before

Correspondence: Kaoru Fujinami
Laboratory of Visual Physiology, National Institute of Sensory Organs, National Tokyo Medical Center, 2-5-1 Higashigaoka, Meguro-ku, Tokyo 152-8902, Japan
Tel +81 3 3411 0111
Fax +81 3 3411 0185
Email kfj21kfj21kfj21@kmf.biglobe.ne.jp

submit your manuscript | www.dovepress.com
Dovepress
http://dx.doi.org/10.2147/OPTH.S75558

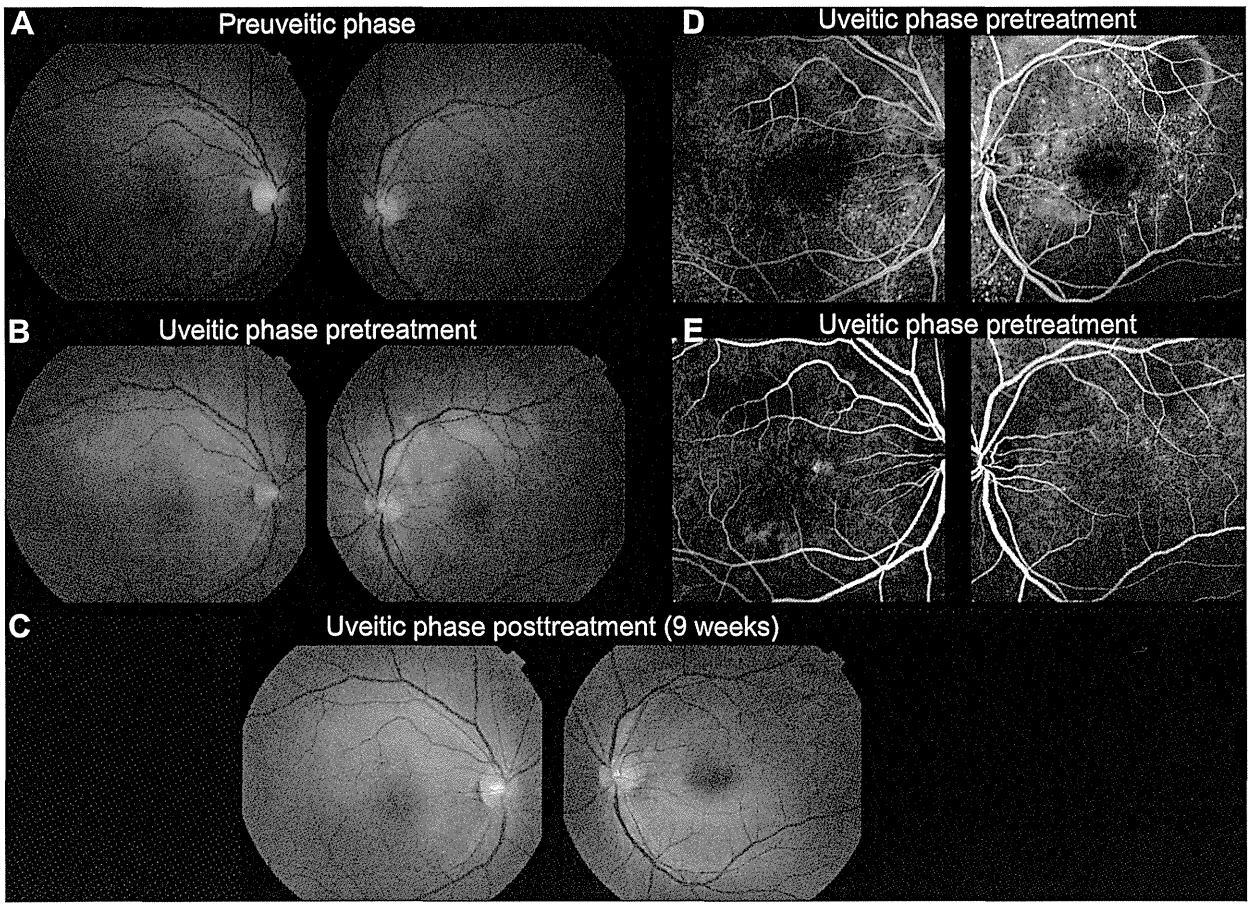

Figure 1 Fundus photographs, fluorescein angiograms, and indocyanine green angiograms of a case with Vogt–Koyanagi–Harada disease (subject 1).
Notes: (**A**) Fundus photography at preuveitic phase (1 year before the onset of uveitis) showed subtle RPE disturbance at the fovea in the right eye with normal findings in the left eye. (**B**) At the onset, fundus photography revealed bilateral multifocal exudative retinal detachments throughout the posterior pole in each eye, with the subtle RPE disturbance unchanged in the right eye. (**C**) Nine weeks after treatment, the exudative detachments had resolved in each eye. (**D**) Fluorescein angiography at the onset demonstrated multiple punctate hyperfluorescent lesions and multilobular pools of subretinal dye in each eye. (**E**) Indocyanine green angiography at the onset identified multiple hypofluorescent spots in each eye with a hyperfluorescent lesion at the superior nasal fovea.
Abbreviation: RPE, retinal pigment epithelial.

the onset of VKH due to symptoms of a floater and visual disturbance demonstrated a dome-shaped posterior protrusion of the RPE and outer retinal layers into the choroidal cavity (ie, conforming FCE) at the fovea in the right eye. SD-OCT at the uveitic phase identified multiple bilateral sensory retinal detachments, with the FCE now involving only the RPE (ie, nonconforming FCE). Nine weeks after the treatment, the nonconforming FCE returned into a conforming pattern.

The FCE pattern and its alteration during treatment of the case with VKH were compared to those of four subjects with FCE associated with other chorioretinal conditions (Figure 3). This comparison group consisted of two patients with age-related macular degeneration (AMD; subjects 2 and 3), one subject with a macular hole (MH; subject 4), and one asymptomatic individual (subject 5). Treatment with intravitreal ranibizumab injections and vitrectomy had been performed in the patients with AMD and MH, respectively. A conforming FCE was observed in three patients (subjects 2, 3, and 5) and pattern alteration from nonconforming to conforming FCE was found after treatment in one subject (subject 4). In the two subjects with AMD, a hyperreflective material around the FCE was absorbed, resulting in a well-demarcated conforming FCE after treatment.

Discussion

A detailed clinical course of FCE at the fovea was documented in a case with VKH disease. SD-OCT images obtained at the preuveitic, uveitic, and posttreatment phase suggested the preexistence of FCE before the onset of VKH, and the FCE pattern change (from conforming to nonconforming pattern during the period of choroidal inflammation) was observed during the follow-up.

The FCE identified at the preuveitic phase in our case supported the congenital/acquired posterior pole

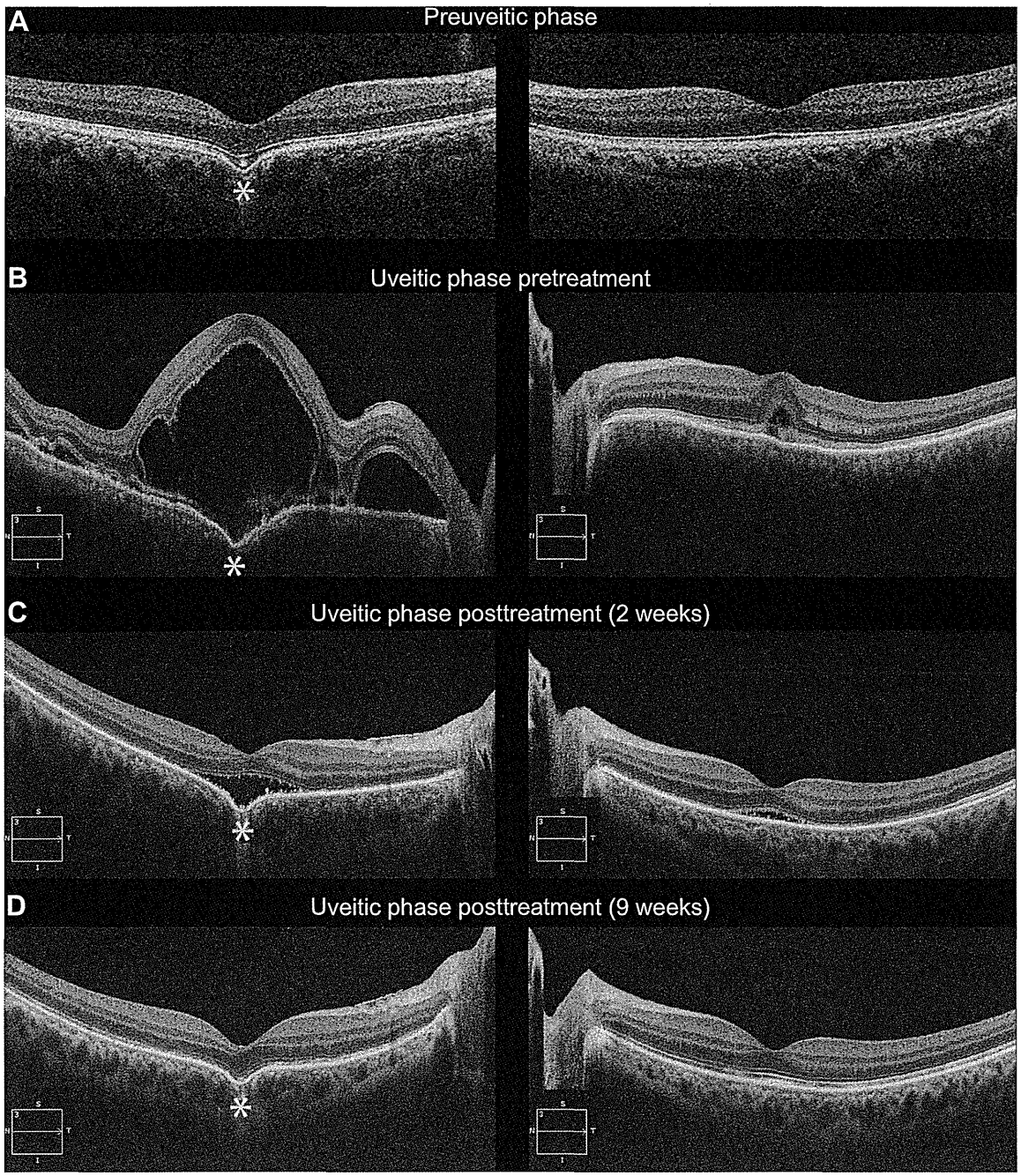

Figure 2 Serial spectral-domain optical coherence tomographic images of a case with Vogt–Koyanagi–Harada disease (subject 1).
Notes: (**A**) Spectral-domain optical coherence tomography at the preuveitic phase (1 year before the onset) showed a dome-shaped posterior protrusion of the hyperreflective bands of the RPE and outer retinal layers into the choroidal cavity (ie, conforming pattern of FCE) at the fovea in the right eye, with normal findings in the left eye (FCE asterisked). (**B**) At the onset, multiple bilateral sensory retinal detachments were demonstrated in each eye, with the FCE involving only the RPE (ie, nonconforming FCE) (FCE asterisked). (**C**) Two weeks after treatment, the serous detachments had partially resolved, with residual subretinal fluid at the fovea in each eye, with a nonconforming FCE at the right fovea (FCE asterisked). (**D**) Nine weeks after treatment, the serous detachments had entirely resolved, resulting in the reappearance of a conforming FCE at the right fovea (FCE asterisked).
Abbreviations: FCE, focal choroidal excavation; RPE, retinal pigment epithelium.

malformation, as previously suggested.[1,4,9,11,12] On the other hand, Hashida et al[13] speculated that a direct pressure effect on the choroidal layer by subretinal fibrin disrupted the choroidal integrity and focal choroidal atrophy/thinning following inflammation and resulted in a formation of FCE in a case with VKH.[4,7,13] Although such a remarkable subretinal fibrin was not detected, the association between the FCE formation and choroidal inflammation could not be excluded entirely in our case, considering other possible subclinical inflammatory events prior to this disease history.

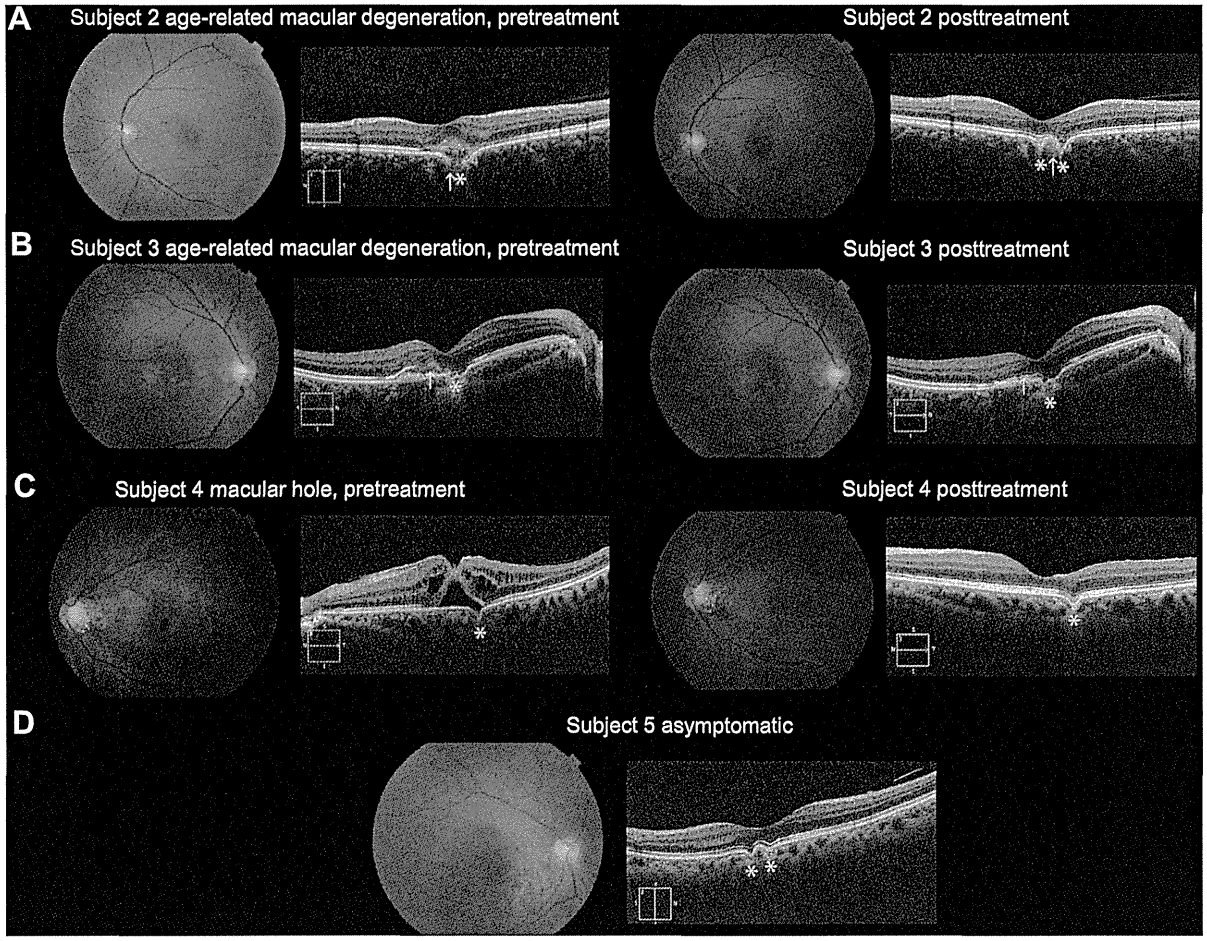

Figure 3 Fundus photographs and spectral-domain optical coherence tomographic images of four cases with focal choroidal excavation (subjects 2, 3, 4, and 5).
Notes: (**A**) Subject 2 (54-year-old man with age-related macular degeneration): Fundus photography at onset showed subtle RPE disturbance at the fovea, and SD-OCT demonstrated an FCE filled with a hyperreflective material (left; FCE asterisked; material arrowed). After treatment with intravitreal ranibizumab injections, a juxtafoveal hypopigmented spot was seen surrounded by RPE disturbance; the hyperreflective material in the FCE had been absorbed and a well-demarcated conforming FCE was observed (right; FCEs asterisked; absorbed material arrowed). (**B**) Subject 3 (67-year-old man with age-related macular degeneration): Fundus photography at onset revealed subtle RPE disturbance at the fovea surrounded by a hypopigmented area at the macula; SD-OCT detected a FCE and subretinal hyperreflective material above the irregular RPE (left; FCE asterisked; material arrowed). After intravitreal ranibizumab injections, the fundus appearance had not changed and a conforming FCE was clearly observed with the irregular RPE (right; FCE asterisked; absorbed material arrowed). (**C**) Subject 4 (55-year old woman with macular hole): Fundus photography showed a hyperreflective membrane at the macula with RPE loss at the fovea; SD-OCT demonstrated an impending MH with retinoschisis and a juxtafoveal nonconforming FCE (left; FCE asterisked). After vitrectomy, the MH had sealed following removal of vitreomacular traction and a conforming FCE was observed (left; FCE asterisked). (**D**) Subject 5 (72-year-old asymptomatic woman): Fundus photography revealed no abnormalities and SD-OCT detected conforming FCEs at the fovea (left; FCEs asterisked).
Abbreviations: FCE, focal choroidal excavation; MH, macular hole; RPE, retinal pigment epithelium; SD-OCT, spectral-domain optical coherence tomography.

An alteration of the FCE pattern observed in VKH was also found in the comparison group with other chorioretinal conditions. In subject 4 with an MH, the nonconforming FCE at presentation associated with vitreomacular traction changed to conforming FCE after treatment. In two subjects with AMD, a hyperreflective material around the FCE was observed to be absorbed, resulting in a well-demarcated conforming FCE via treatment (subjects 2 and 3). These findings suggest that the cavity within FCE can be filled with subretinal fluid associated with inflammation and exudative material generated by choroidal neovascularization. The decreased adhesion within the FCE between RPE and photoreceptor could complicate MHs. Given the proximity between the FCE and the active lesions, the involved retina around the active lesion may well show disorganization of retinal layers in the pathological process; then the conforming pattern is hard to maintain, unsurprisingly. In addition, it is possible that the cavity within FCE may potentially accelerate the pathophysiological changes of chorioretinal disorders.

Acknowledgments

This research was supported in part by research grants from the Ministry of Health, Labor and Welfare, Japan and Grant-in-Aid for Scientific Research from Japan Society for the

Promotion of Science. KF is supported by a Grant-in-Aid for Young Scientists (B) of the Ministry of Education, Culture, Sports, Science and Technology (Japan). The sponsor or funding organization had no role in the design or conduct of this research.

Disclosure

The authors have no proprietary or commercial interest in any materials discussed in this article. The authors report no other conflicts of interest in this work.

References

1. Jampol LM, Shankle J, Schroeder R, Tornambe P, Spaide RF, Hee MR. Diagnostic and therapeutic challenges. *Retina*. 2006;26(9):1072–1076.
2. Wakabayashi Y, Nishimura A, Higashide T, Ijiri S, Sugiyama K. Unilateral choroidal excavation in the macula detected by spectral-domain optical coherence tomography. *Acta Ophthalmol*. 2010;88(3):e87–e91.
3. Margolis R, Mukkamala SK, Jampol LM, et al. The expanded spectrum of focal choroidal excavation. *Arch Ophthalmol*. 2011;129(10):1320–1325.
4. Ellabban AA, Tsujikawa A, Ooto S, et al. Focal choroidal excavation in eyes with central serous chorioretinopathy. *Am J Ophthalmol*. 2013;156(4):673–683.
5. Obata R, Takahashi H, Ueta T, Yuda K, Kure K, Yanagi Y. Tomographic and angiographic characteristics of eyes with macular focal choroidal excavation. *Retina*. 2013;33(6):1201–1210.
6. Say EA, Jani PD, Appenzeller MF, Houghton OM. Focal choroidal excavation associated with polypoidal choroidal vasculopathy. *Ophthalmic Surg Lasers Imaging Retina*. 2013;44(4):409–411.
7. Lee CS, Woo SJ, Kim YK, et al. Clinical and spectral-domain optical coherence tomography findings in patients with focal choroidal excavation. *Ophthalmology*. 2014;121(5):1029–1035.
8. Or C, Forooghian F. Vitelliform focal choroidal excavation. *Ophthalmic Surg Lasers Imaging Retina*. 2014;45 Online:e26–e28.
9. Xu H, Zeng F, Shi D, Sun X, Chen X, Bai Y. Focal choroidal excavation complicated by choroidal neovascularization. *Ophthalmology*. 2014;121(1):246–250.
10. Parodi MB, Zucchiatti I, Fasce F, Bandello F. Bilateral choroidal excavation in best vitelliform macular dystrophy. *Ophthalmic Surg Lasers Imaging Retina*. 2014;45 Online:e8–e10.
11. Suzuki M, Gomi F, Hara C, Sawa M, Nishida K. Characteristics of central serous chorioretinopathy complicated by focal choroidal excavation. *Retina*. 2014;34(6):1216–1222.
12. Lee JH, Lee WK. Choroidal neovascularization associated with focal choroidal excavation. *Am J Ophthalmol*. 2014;157(3):710–718.e1.
13. Hashida N, Fok A, Nishida K. Choroidal excavation in vogt-koyanagi-harada disease. *Case Rep Ophthalmol*. 2014;5(2):222–225.

Occult macular dystrophy

Yozo Miyake 1,2
Kazushige Tsunoda 2,* Phone+81-3-3411-0111
Emailtsunodakazushige@kankakuki.go.jp
1Aichi Medical UniversityNagakute, Aichi480-1195Japan
2Division of Vision ResearchNational Institute of Sensory Organs2-5-1 Higashigaoka, Meguro-kuTokyo152-8902Japan

Abstract

Occult macular dystrophy (OMD) was first reported in 1989 as a hereditary macular disease without visible fundus abnormalities. Patients with OMD are characterized by a progressive decrease of visual acuity but have normal fundus and fluorescein angiograms with both the rod and cone components of the full-field electroretinograms (ERGs) essentially normal. However, the focal macular ERGs and multifocal ERGs are severely attenuated. These findings indicate that the retinal dysfunction is confined to the macula. Optical coherence tomography (OCT) has shown structural changes in the outer nuclear and/or photoreceptor layers. Genetic analyses of OMD pedigrees have identified dominant mutations in the *RP1L1* gene. However, the same mutations were not detected in sporadic cases, suggesting that several independent mutations can lead to the OMD phenotype. The purpose of this paper is to review the history of OMD, the visual functions determined psychophysically, ERG findings, OCT characteristics and genetic findings in patients with OMD.

Keywords
Occult macular dystrophy
Focal macular ERG
Multifocal ERG
Optical coherence tomography
RP1L1 gene

Introduction

At the beginning of the 20th century, three well-known retinal diseases were identified by Japanese ophthalmologists, i.e., Oguchi disease [1], Takayasu disease [2] and Harada disease [3]. Each of these diseases has unique fundus findings, and their discoveries coincided with the development of new fundus examination techniques.

There are several hereditary retinal diseases in which fundus findings are normal and provide little information for diagnosis. In these diseases, the characteristics of the electroretinograms (ERGs) play an important role in the diagnosis. For example, congenital stationary night blindness (CSNB) with normal fundus findings is classified into complete and incomplete types by a detailed analysis of the full-field ERGs [4]. Although there were questions as to whether these two types of CSNB were different clinical entities, genetic analyses proved that the complete and incomplete types of CSNB were indeed different clinical entities [5–9]. Eyes with the cone dysfunction syndrome, e.g., cone dystrophy [10] and rod [11] or blue cone monochromacy [12], also have a normal fundus, and only the findings of full-field ERGs can lead to a correct diagnosis.

The history of occult macular dystrophy (OMD) is slightly different. Patients were found with a progressive decrease in the visual acuity and essentially normal fundus and fluorescein angiographic findings [13–15]. In contrast to the CSNB and cone dysfunction syndrome cases, these patients had normal full-field ERGs. Only after the development of the focal macular ERG [16–20] techniques was it found that these patients had a depression of the macular function. This indicates that the retinal dysfunction is confined only to the macula.

The first account of OMD was published in 1989 under the title "Hereditary macular dystrophy without visible fundus abnormality" [13]. Thereafter, several depictions of patients with similar phenotypes were published [14], and this clinical condition was named, "occult macular dystrophy" in 1996. The term occult was used to mean that the cause of the dystrophy was "hidden from sight".

At first, OMD could only be diagnosed by the results of both full-field ERGs and focal macular ERGs. After multifocal ERGs (mfERGs) were developed [21], patients diagnosed with OMD following the full-field and focal macular ERG findings were found to have a reduction of the amplitudes of the mfERGs recorded from the central areas. With the widespread use of mfERGs, patients worldwide were diagnosed with OMD based on the findings of mfERGs [22–24].

With the development and refinement of optical coherence tomography (OCT), eyes diagnosed with OMD by electrophysiological findings were found to have structural abnormalities in spite of the normal appearance of

the macula by ophthalmoscopy [25–30].

The hereditary mode of OMD has been shown to be autosomal dominant in many patients whereas others were classified as sporadic. In 2010, genetic studies detected mutations in the retinitis pigmentosa 1-like 1 (*RP1L1*) gene in an eye with autosomal dominant OMD [31].

The important point clinically is that OMD is not a rare disease and that more advanced electrophysiological and imaging techniques are needed to make a correct diagnosis. Thus, patients with reduced visual acuity and a normal fundus may be misdiagnosed with various diseases other than OMD.

Here we present the history of the discovery of OMD, detailed clinical characteristics, electrophysiological characteristics and genetic information of eyes with OMD.

History of occult macular dystrophy (OMD)

In 1989, Miyake et al. reported on three patients from two generations of the same family with poor visual acuity. The fundi of the three patients appeared normal by ophthalmoscopy and fluorescein angiography, even in the older patient, and the results of full-field electroretinograms were also normal for both the cone and rod components. However, the amplitudes of the focal macular ERGs were severely reduced. This paper was published under the title, "Hereditary macular dystrophy without visible fundus abnormality". The diagnosis of OMD in these patients was made only after the development of the focal macular ERG.

Development of focal macular ERG techniques

The principle of recording focal macular ERGs includes presenting a small stimulus to the macula and recording the response elicited from this area. Several investigators had tried to obtain responses from the macula alone, but the results were not satisfactory because of the strong effect of stray light. Layer-by-layer analysis by recording many components of cone ERG, necessary for routine clinical examinations, was not possible, either. To minimize the effects of stray light responses, background illumination must be used to suppress the sensitivity of the area surrounding the stimulus. It is also important to monitor the location of the stimulus on the fundus during the recording to be certain that only the macula is being stimulated. This is especially true for eyes with macular diseases with a central scotoma.

In 1988, a comprehensive system for recording focal macular ERGs was

developed by modifying an infrared television fundus camera. With this system, the a-waves, b-waves, d(off)-waves, oscillatory potentials, photopic negative responses (PhNR) [32], and 30 Hz flicker responses could be accurately recorded exclusively from the human macula (Fig. 1) [16, 17, 19]. Using this system, a layer-by-layer analysis of the retina with different macular diseases could be obtained. The first diagnosis of an OMD patient and detail analyses of the pathogenesis of many OMD patients were accomplished with this system.

Fig. 1

Components of the focal macular ERGs recorded in a normal subject [16, 19]. The ON and OFF responses recorded with 1-Hz frequency (*top*); *a*-wave and *b*-wave, oscillatory potentials (OPs), and photopic negative response (PhNR) recorded with 5-Hz stimulus frequency (*middle*); and 30-Hz flicker responses (*bottom*) are shown. *TC* time constant

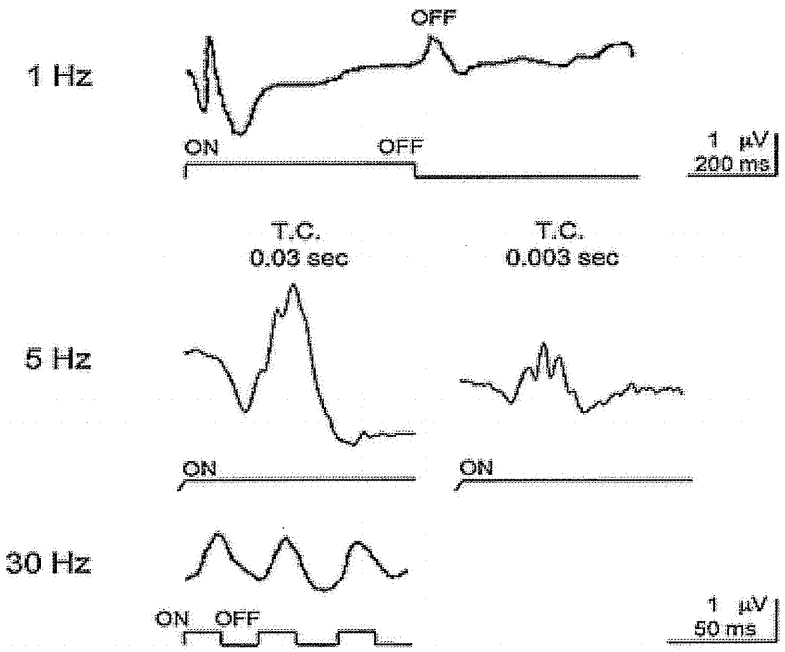

Development of multifocal ERGs

In 1992, 3 years after OMD was firstly reported, a new technique termed multifocal ERG (mfERG) was developed by Sutter and Tan [21]. To record the mfERGs, the retina is stimulated with an array of hexagonal stimuli generated on a computer monitor. The sizes of the hexagons are scaled with eccentricity to elicit approximately equal amplitude responses at all locations. Each hexagon has a 50 % chance of being bright at each frame

change. The pattern appears to flicker randomly, but each element follows a fixed, predetermined *m*-sequence so the overall luminance of the screen over time is relatively stable. By correlating the continuous ERG signals with the on and off phases of each stimulus element, the focal ERG signals associated with a specific hexagonal element is recorded. An array of the 103 focal responses of the multifocal ERG and a topographic map of the amplitude of the ERG at each locus are shown in Fig. 2. With this method, ERGs can be recorded simultaneously from multiple focal retinal locations during a single recording session using cross-correlation techniques. Since its introduction it has been used worldwide and many patients with OMD were correctly diagnosed by analyzing the mfERGs [22–24].

Fig. 2

Stimulus matrix (*top*), multifocal ERG responses (*middle*), and a topographic plot of the amplitudes (*bottom*) of standard multifocal ERG recordings from a normal subject. The *arrow* in the *middle* shows a response from the area around the optic disc

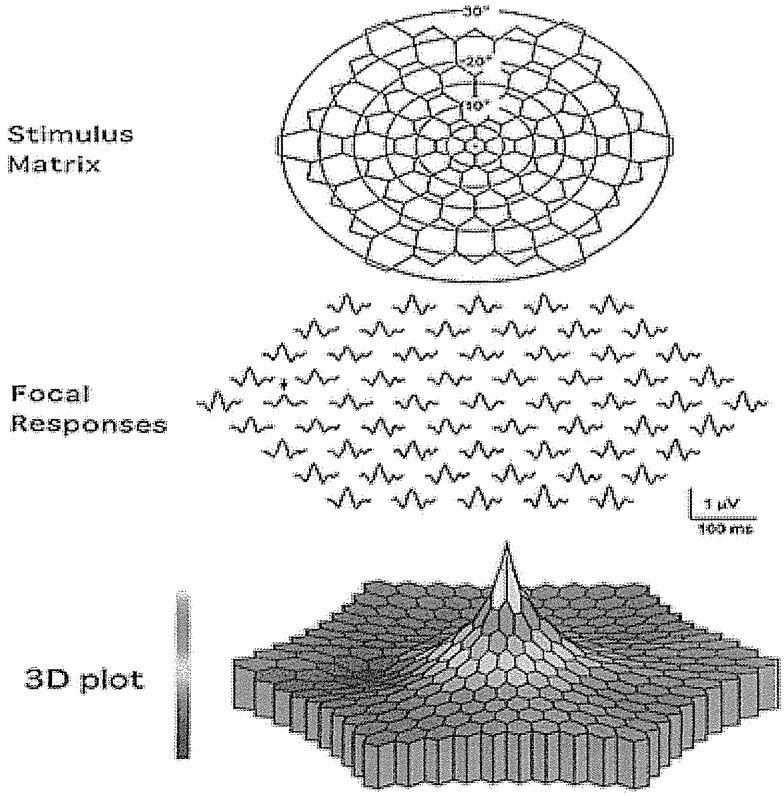

Age and visual acuity of OMD patients

The age at which a patient with OMD recognizes a decrease of vision varies

widely from as young as 6 to 60 years old. In a study of a large family with thirteen OMD patients (six men and seven women) carrying the p.Arg45Trp mutation (Fig. 3), the age at the onset of visual difficulties varied from 6 to 50 years with a mean of 27.3 ± 15.1 years. The average age at the final examination was 57.2 ± 22.1 years [30]. The duration of the continuous decrease in the visual acuity varied from 10 to 30 years (mean 15.6 ± 7.7) in 16 eyes of 9 adult patients. After this period, the vision did not decrease. All of the patients were affected in both eyes, and the onset was the same in the two eyes except for four patients (cases 1–4) [30]. One patient (case 1) first noticed a decrease in her visual acuity OS at age 50 years, and she still did not have any subjective visual disturbances OD 30 years later. However, a clear decrease in the mfERG in the macular area was detected OU.

Fig. 3

Pedigree of a family with OMD. All thirteen patients had the *RP1L1* gene mutation (p.Arg45Trp). The proband is indicated by the *arrow*. ~~Reprinted with permission from~~ the ~~*American Journal of Ophthalmology*~~

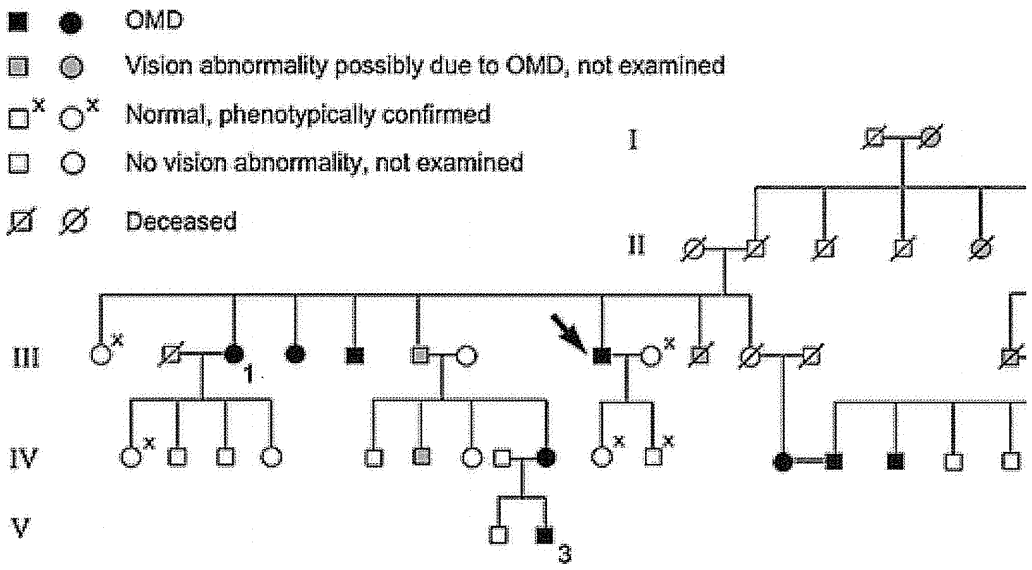

The BCVA of OMD patients is occasionally normal or only slightly affected, although the response of focal macular ERG is reduced. In such cases, OCT can demonstrate a small normal morphological region at the fovea.

The distribution of the visual acuities and age at the initial visit in 33 patients (22 men and 15 women) examined at Nagoya University is shown

in Fig. 4 [15]. This graph contains patients from different families, but not all these patients had gene analyses performed. The graph shows that some of the patients had normal visual acuity despite their focal macular ERGs being definitely reduced. There is no obvious correlation between the age at the initial visit and the visual acuity.

Fig. 4

Distribution of visual acuities (*x*-axis) versus age (*y*-axis) in eyes with OMD [15]. Note that some patients have normal visual acuity. Adapted with permission from Miyake Y. 'Electrodiagnosis of retinal diseases', Tokyo: Springer-Verlag; 2006

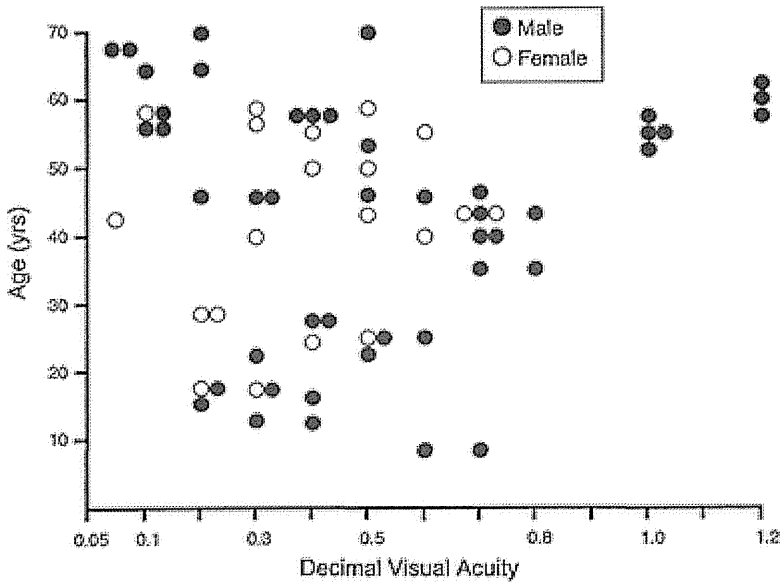

Fundus findings and fundus autofluorescence images

Three fundus photographs and fluorescein angiograms from one family with OMD are shown in Fig. 5 [13]. They are essentially normal. The fundus autofluorescence (AF) images were also essentially normal in the entire posterior pole (Fig. 6a). However, some cases (~50 % of patients with the *RP1L1* mutation) have been shown to have a circular area with increased AF signal at the fovea [33]. This area of increased AF is very faint in some cases (Fig. 6b arrow) and more apparent in others (Fig. 6c, arrow). These findings imply that the primary lesion of OMD is in the photoreceptors rather than the RPE. The AF abnormalities in eyes with OMD are very different from other macular dystrophies and cone-rod dystrophies, which have distinctive patterns of AF. The relationship

between duration of the disease and intensity of the increased AF signal has not been confirmed.

Fig. 5

Fundus photographs (*left*) and fluorescein angiograms (*right*) of three patients with OMD from a single family [15]. Cases 1, 2, and 3 are a 29-year-old woman, a 19-year-old man, and a 55-year-old-man, respectively. Case 3 is the father of cases 1 and 2. All three patients had the *RP1L1* gene mutation [31]. Adapted with permission from Miyake Y. 'Electrodiagnosis of retinal diseases', Tokyo: Springer-Verlag; 2006

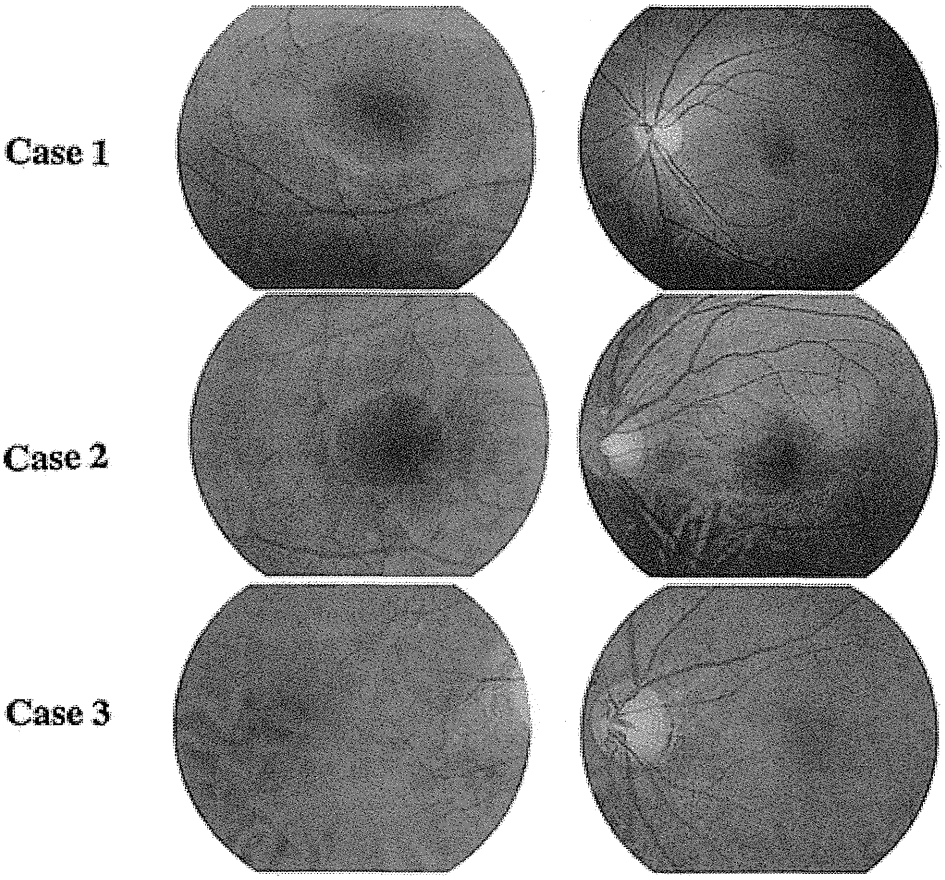

Fig. 6

Fundus autofluorescence (AF) images in three OMD patients with *RP1L1* mutation (p.Arg45Trp, heterozygous). **a** A 32-year-old woman with normal AF image. **b** A 30-year-old man showing faint increased AF at the fovea (*arrow*). **c** A 71-year-old woman showing a mildly increased AF signal at

the fovea without a distinct border (*arrow*). All the AF images were recorded with a 488-nm wavelength using a barrier filter for the detection of emitted light above 500 nm (HRA2; Heidelberg Engineering, Heidelberg, Germany)

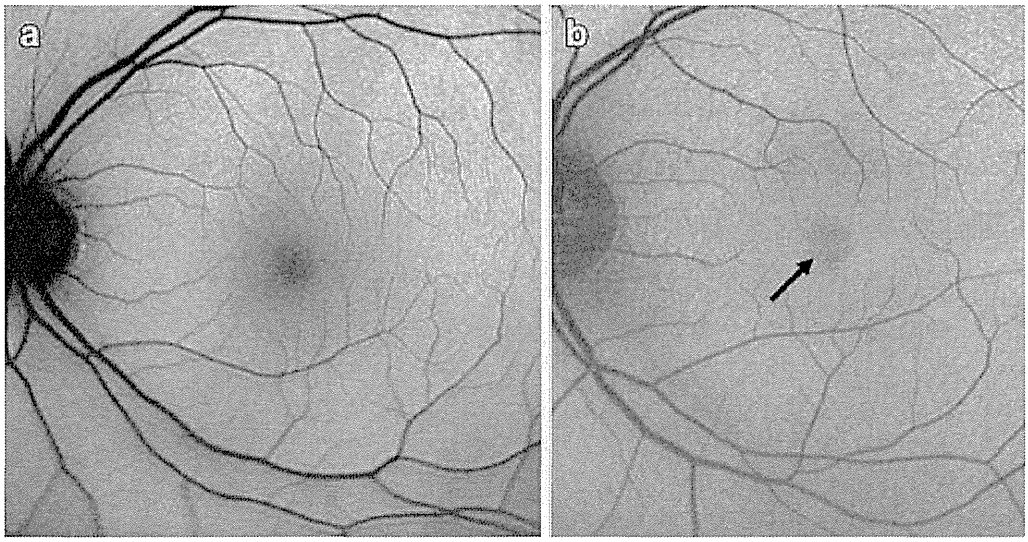

Electroretinograms (ERGs)

The full-field ERGs recorded with the ISCEV standard protocol are normal for both the rod and cone components in patients with OMD; however, some patients may show slightly reduced cone ERGs. The amplitudes and implicit times of the focal macular ERGs are markedly reduced and delayed, and the mfERGs are reduced in the central areas. The findings of full-field ERGs and focal macular ERGs recorded with three diameter spot sizes (5°, 10°, and 15°) in a typical patient with OMD are shown in Fig. 7.

Fig. 7

Full-field ERGs (*upper*) and focal macular ERGs elicited by three spots of different sizes (5°, 10°, 15°in diameter) (*lower*) in an OMD patient

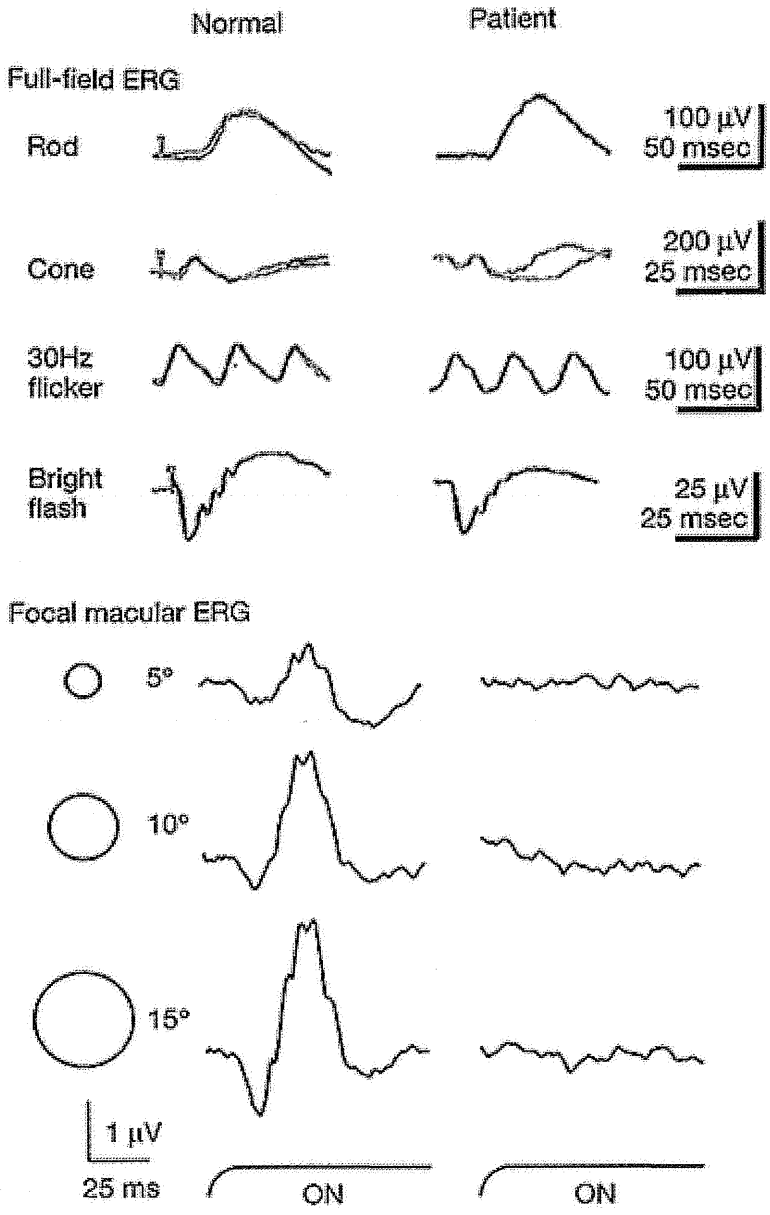

Many OMD patients have non-detectable focal macular ERGs when the stimulus spot is small. However, when the stimulus spot is relatively large (10° or 15° in diameter), a response is recordable but is significantly smaller than normal (Fig. 8). The waveform of the response is often a small *a*-wave with a relatively large *b*-wave [23]. The cone ERGs recorded with long duration stimuli are classified as having a depolarizing pattern response which is similar to that recorded when the ON-bipolar cell is predominantly functioning [34]. These results suggest that the OFF visual pathway is more severely affected in the macula in eyes with OMD.

Fig. 8